



## Article

# Dual-Mode Stretchable Sensor Array with Integrated Capacitive and Mechanoluminescent Sensor Unit for Static and Dynamic Strain Mapping

Song Wang <sup>1,†</sup>, Xiaohui Yi <sup>2,†</sup> , Ye Zhang <sup>2</sup>, Zhiyi Gao <sup>2</sup>, Ziyin Xiang <sup>2</sup>, Yuwei Wang <sup>2</sup>, Yuanzhao Wu <sup>2</sup>, Yiwei Liu <sup>2</sup>, Jie Shang <sup>2,\*</sup>  and Run-Wei Li <sup>2,\*</sup>

<sup>1</sup> Faculty of Electrical Engineering and Computer Science, Ningbo University, Ningbo 315211, China

<sup>2</sup> CAS Key Laboratory of Magnetic Materials and Devices, Ningbo Institute of Materials Technology and Engineering, Chinese Academy of Sciences, Ningbo 315201, China

\* Correspondence: shangjie@nimte.ac.cn (J.S.); runweili@nimte.ac.cn (R.-W.L.)

† These authors contributed equally to this work.

**Abstract:** Electronic skin (e-skin) has the potential to detect large-scale strain, which is typically achieved by integrating multiple strain sensors into an array. However, the latency and limited resolution of sensing have hindered its large-scale sensing applications. Here, we have developed a high-resolution detection sensing system capable of detecting static and dynamic strain with a simple fabrication process by combining capacitive and mechanoluminescent (ML) sensor units. An elastic polydimethylsiloxane (PDMS) composite film doped with ZnS:Cu and BaTiO<sub>3</sub>(BT) particles are fabricated as the functional film of the capacitive sensor. In contrast, the transparent electrode was fabricated on the surface of the as-prepared film. By incorporating BT nanoparticles into the elastic substrate, the ML intensity of the ZnS:Cu was improved up to 2.89 times that without BT addition, and the sensitivity of the capacitive sensor was increased as well. The capacitive part of the sensor presented a GF of 0.9 and good stability, while the ML part exhibited excellent performance, making it suitable for both static and dynamic sensing. Furthermore, the strain sensor integrated by 10 × 10 sensing units is demonstrated to detect large-scale strain with high resolution. Moreover, finger joint strain distribution tracking is achieved by attaching the strain sensor unit to the finger joint. With these characteristics, the e-skin may have great potential for bio-motion monitoring and human-computer interaction applications.

**Keywords:** e-skin; mechanoluminescence; strain sensor; dynamic and static sensing



**Citation:** Wang, S.; Yi, X.; Zhang, Y.; Gao, Z.; Xiang, Z.; Wang, Y.; Wu, Y.; Liu, Y.; Shang, J.; Li, R.-W. Dual-Mode Stretchable Sensor Array with Integrated Capacitive and Mechanoluminescent Sensor Unit for Static and Dynamic Strain Mapping. *Chemosensors* **2023**, *11*, 270. <https://doi.org/10.3390/chemosensors11050270>

Academic Editor: Qingjun Liu

Received: 7 April 2023

Revised: 27 April 2023

Accepted: 30 April 2023

Published: 2 May 2023



**Copyright:** © 2023 by the authors. Licensee MDPI, Basel, Switzerland. This article is an open access article distributed under the terms and conditions of the Creative Commons Attribution (CC BY) license (<https://creativecommons.org/licenses/by/4.0/>).

## 1. Introduction

Artificial electronic skin (e-skin), composed of mechanically flexible and stretchable sensors, is designed to imitate the human somatosensory system by detecting and converting various stimuli to analyzable signals for potential applications in health monitoring, human-computer interaction, and sports performance monitoring [1–3]. The stretchable strain sensor can be integrated into e-skin for monitoring physiological functions and body motions associated with different levels of strain, such as blood pressure [4], joint bending [5], and muscle deformation [6]. When stretchable strain sensors are attached to human skin for health or motion monitoring, the e-skin should have a stretchability larger than 30%, known as the maximum skin stretchability generated by daily human motion. Therefore, developing a sensing system with fast response, good stability, highly sensitive, high spatial resolution, and energy efficiency is necessary for imitating the extremely complex somatosensory sensing model [7]. Very recently, a few progresses have been reported in developing novel designed strain sensors employing various physical effects such as capacitive [8], piezoresistive [9], piezoelectric [10], and triboelectric [11] sensing

mechanisms. Among these sensors, the capacitance-based strain sensor has excellent performance of small hysteresis, negligible temperature fluctuations and highly-stability, which attracted extensive research interests [12]. However, integrating multiple capacitive sensing units into arrays creates a serious challenge as the number of sensors increases due to various issues such as complex wiring and time delay of external read-out circuitry [13–16]. Moreover, capturing the whole process of the gesture or deformation of the skin during fast body movement requires high data acquisition frequency and a complex calculation process for analyzing the target information, for example, the explosive muscle power, which will induce high energy consumption, reducing the battery endurance time.

To address this challenge, a practical strategy is to introduce other fast response sensing signals into a single device for compensation for the shortcomings in the capacitive sensor arrays. Optical signals have the advantages of fast transmission rate, anti-inference characteristics and low energy consumption readout [17]. Notably, mechanically driven light generation, defined as mechanoluminescence (ML), is observed in a few materials, such as ZnS:Cu powders [18]. The intensity of the ML shows a strong correlation with the applied stress, making it suitable for stress sensing [19]. Over the past few decades, ML-based strain sensing has been developed with great effort. As a result, not only the luminous intensity and sensitivity have been improved [20–23]. Integrated with the self-powered photodetector array, the ML sensor provide an energy-saving approach for long-time biomechanical monitoring applications [24]. Nevertheless, the volatile nature of the ML limits their application, especially for static strain measurement [25].

Enlightened by the capacitive and ML sensing characteristics, elastic polydimethylsiloxane (PDMS) composite film doped with both ZnS:Cu and BaTiO<sub>3</sub>(BT) is fabricated in this work. Based on the as-prepared functional film, a capacitive and ML dual-mode stretchable strain sensor with transparent electrodes is demonstrated. The doping of ZnS:Cu is selected for generating stress-driven luminescence and real-time mapping of dynamic strain. By adding rigid and high dielectric particles BT into the stretchable matrix, stress concentration on the ZnS:Cu particles can be achieved during stretching, enhancing ML intensity with weak stimuli. Moreover, BT particles will also increase the dielectric constant of the composite film and improve the capacitive performance behavior of the sensor. In addition, the stretchable elastomer substrate enables the e-skin to withstand large mechanical deformations. The strain sensor array integrated by 10×10 capacitive sensing units is demonstrated for the capability of detecting large-scale strain with high resolution. Continuous tracking of finger joint strain distribution is achieved by attaching the strain sensor unit to the finger joint. Featuring these characteristics, the e-skin may have great potential for bio-motion monitoring and human-computer interaction applications.

## 2. Materials and Methods

### 2.1. Chemicals and Reagents

Barium Titanate (BaTiO<sub>3</sub>, 99.9% metals basis, <100 nm) and silver nanowire (AgNW, purity: >99.5% solvent: ethanol) were purchased from Aladdin. ZnS:Cu (D502CT) was supplied by Shanghai Keyan Phosphor Technology Co., Ltd. (Shanghai, China). Polydimethylsiloxane (Sylgard 184 Silicone Elastomer) with a curing agent was purchased from Dow Corning. Hydrogen peroxide solution (H<sub>2</sub>O<sub>2</sub>, AR, 70 wt% in H<sub>2</sub>O) was purchased from Aladdin. Silane coupling agent kh-171 (purity: >99%) was purchased from Union Carbide Corporation of America.

### 2.2. Synthesis of Modified BT Particles

The surface modification of BT is mainly divided into two steps. Firstly, BT is refluxed with hydrogen peroxide at 105 °C to graft it with the hydroxyl group. Then the reactants are refluxed with silane coupling agent kh-171, hydrolysis reaction occurs. Finally, the silane coupling agent is grafted on the surface of BT. Thus, vinyl groups are introduced (Figure S1).

### 2.3. Synthesis of PDMS/ZnS:Cu-BT Composite

Mixing modified BT with PDMS precursor fluid and heating at 70 °C, cross-linking reaction occurs between vinyl groups on the surface of modified BT and silicon hydrogen groups in PDMS precursor solution. The modified BT nanoparticles can be adhered to by PDMS macromolecular chains (Figure S2). The functional layer was produced by mixing the PDMS base polymer (Sylgard 184) with the curing agent (Sylgard 184), ZnS:Cu particles and BaTiO<sub>3</sub> nanoparticles, with a weight ratio of 10:2:10:0–0.3.

### 2.4. Characterization

**Device characterization:** The SEM images of the surface morphology of AgNW/PDMS and cross-sectional morphology were acquired from the scanning electron microscope (Sirion200). The EDS data were obtained from field-emission scanning electron microscopy (Hitachi S-4800). Strain distribution was generated by the optical test part of the non-contact strain-electrical-thermal test system (ARAMIS 3D 12M). In the fatigue property test, the cyclic strain was produced by a mechanical motion platform.

**ML Measurements:** A homemade measuring system was built to collect ML intensity, universal material testing machine (Instron 5943, Boston, MA, USA) applied the strain levels. Light emissions were collected from the contact point by a photon counter and a photon counting head (Hamamatsu C8855-01, Hamamatsu, Japan).

**Capacitance Measurements:** An impedance analyzer (HIOKI, IM 3570, Ueda, Japan) was used for capacitance signal acquisition.

## 3. Results and Discussion

### 3.1. Conceptual Illustration of Dual-Mode e-Skin

As shown in Figure 1a, the structure of the sensing array is a typical sandwich structure, with an outer transparent electrode clamping a middle functional layer. The functional layer serves as both a dielectric layer for the capacitive sensor and a light-emitting layer for generating optical signals driven by the stress in the layer.

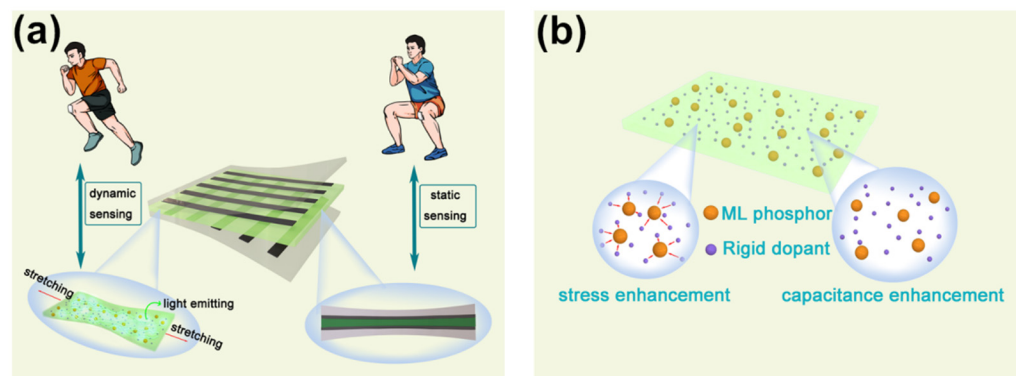


**Figure 1.** Conceptual illustration of dual-mode e-skin. (a) Structure schematic of the e-skin. An ML layer is sandwiched between two stretchable transparent AgNW/PDMS electrodes—an illustration of the different deformation of the e-skin with the different sensing modes. Dynamic strain corresponds to light intensity (left), static strain, and capacitance value. (b) The schematic illustration of enhancement of stress and capacitance by nanoparticle-doped matrix.

The electrodes are located on both sides of the functional layer. The rows and columns of the electrode array are perpendicular to each other, forming capacitors. According to the capacitance formula

$$C = \epsilon_0 \epsilon_r \frac{s}{d} \quad (1)$$

where  $\epsilon_0$  is the permittivity of air,  $\epsilon_r$  represents the dielectric constant of the dielectric material,  $s$  represents the capacitive area,  $d$  represents the distance between the electrodes.

When the e-skin is subjected to strain, the area of the functional materials between the top and bottom electrodes in the capacitor increases and the distance between the electrodes decreases. Thus, the capacitance value increases. The change in the capacitance value is highly correlated with the strain. When the capacitive sensor array is applied to sense strain variation of the skin around bending joints or contracting muscle during fast motion such as running, a huge amount of data will generate depending on the units of sensor integrated and the frequency of data acquisition. The wearable electronic device may not afford this sensing approach and suffers from low battery usage time and slow reaction. Therefore, the capacitance value can be used to accurately measure the strain of the e-skin, allowing for precise monitoring of the static strain.

When the functional layer is stressed, the elastic matrices can transmit stress or strain to inner ML phosphor particles and trigger elastic ML [26]. The intensity of the ML produced from the functional layer is affected by stress, strain, and rate, and within a certain range, it changes with the change of these three factors, thus enabling the ability for strain sensing. In addition, it is noteworthy that ML possesses the property of excellent dynamic response (<10 ms) as well as high resolution [19]. Therefore, the ML layer is expected to be utilized for dynamic sensing and visualization of large-scale strain.

However, the elastic deformation of flexible materials buffers the stress or strain acting on rigid phosphor microparticles, preventing the triggering of obvious ML. As shown in Figure 1b, by surface treating the BT rigid nanoparticles, the BT nanoparticles can tightly adhere to the PDMS macromolecular chains. After modification with a silane coupling agent, BT and PDMS form O-Si chemical bonds, which permits the uniform dispersion of BT particles in the PDMS matrix and allows for the stress induced in the straining process to be transmitted from the PDMS matrix to the ML particles through BT, thus producing stronger ML. Additionally, BT, as a high dielectric material (the dielectric constant of BT is much greater than that of ML particles ZnS:Cu used in this paper), can also improve the electrical performance of the capacitive sensor.

### 3.2. Fabrication Process from the Functional Layer to the e-Skin

The preparation of the functional layer is shown in the upper part of Figure 2. First, the modified BT was added to the PDMS precursor solution. The vinyl groups on the surface of the modified BT particles react with the PDMS precursor solution by cross-linking reaction, which enables the BT to be grafted tightly to the molecular chain of PDMS. After 8 h of stirring at 60 °C, ZnS:Cu particles and curing agent were added. Continue stirring for 10 min. Finally, the solution was poured into the prepared mold and cured to obtain the functional layer film, as shown in Figure 2. As the strain or press is applied, the doped BT nanoparticles can transfer the stress to the microparticles and achieve intense ML under weak stimuli. The lower part of Figure 2 shows the preparation process of the sensor array.

To simulate the flexibility and stretchability of biological skin and ensure effective light emission of the functional layer, manufacturing high-performance stretchable transparent electrodes is essential. An ideal candidate is a flexible AgNW network embedded in an elastic PDMS film. First, a tape-made mask was attached to the surface of the functional layer to form strip-shaped gaps. Then, the silver nanowire solution was evenly dropped onto the surface using a glue dropper, and parallel rows of silver nanowire electrode arrays were obtained by evaporating alcohol on a heating plate. In the same way, patterned electrode arrays were vertically prepared on the back of the functional layer as bottom electrodes. Finally, PDMS was used to encapsulate the upper and lower surfaces of the functional layer. The simple preparation process of this e-skin has provided a reliable and efficient solution for strain detection.

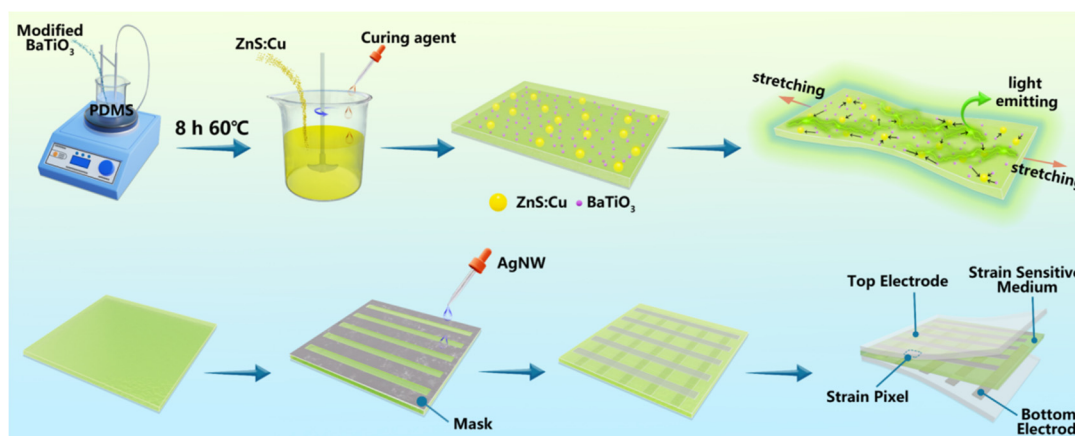


**Figure 2.** Fabrication process from the functional layer to the e-skin with double sensing mode. The above schematic of the preparation process of both the light emitting layer and dielectric layer by introducing BT into ML film. The below schematic of the preparation process of the e-skin integrated transparent electrode and the functional layer.

### 3.3. Characteristics of e-Skin by Nanodoped Matrix Modification

Illustrating the strain sensor structure composed of a functional layer and transparent electrodes is shown in the left part of Figure 3a. The scanning electron microscopy (SEM) image in the right part of Figure 3a shows the AgNW with a diameter of 200 nm distributed evenly on the surface of the functional layer. In our work, PDMS was used to encapsulate the upper and lower surfaces of the functional layer to attach AgNW to the surface of the functional layer strongly. The functional layer is about 400  $\mu\text{m}$  in thickness. It is shown that no aggregation of ZnS:Cu and BT particles is observed in the functional layer. In Figure S3, it is shown in the Energy Dispersive Spectrometer (EDS) image that the Ba and Ti elements are evenly distributed in the matrix, indicating that BT nanoparticles are not agglomerated. The comparison between the PDMS doped with unmodified BT nanoparticles, and modified BT nanoparticles was also made. It is shown that the unmodified BT nanoparticles undergoes agglomeration in the PDMS matrix. This is because the modified BT nanoparticles are covalently grafted with the PDMS molecular chain, while the unmodified BT nanoparticles tend to aggregate due to electrostatic force.

The amount of BT added affects the luminescence and electrical properties of the functional layer. In the following sections, to choose the optimal amount of BT nanoparticles, the effects of BT nanoparticles doping content on the luminescence performance and capacitance performance of the functional layer in the sensor were investigated. First, to examine the effects of BT nanoparticles doping content on electrical properties, the dielectric properties of the functional layers with different doping content of BT nanoparticles were studied by broadband dielectric spectroscopy at room temperature. As a kind of high dielectric ceramic, BT nanoparticles are commonly used as filler to be incorporated into the dielectric layer to enhance the dielectric constant [27]. As shown in Figure 3b, the dielectric constant of the PDMS&ZnS:Cu-BT composites slightly increased compared to the pure PDMS film across a wide frequency range (100 Hz to 1 MHz). The pure PDMS film had a dielectric constant of approximately  $\epsilon_r \sim 3$  at 100 Hz [1]. After adding 10 wt%, 20 wt%, and 30 wt% BT nanoparticles, its dielectric constants rose to 3.7, 4.2, and 4.6 at 100 Hz, respectively. It is demonstrated that the dielectric constant of the PDMS film can be enhanced by incorporating a high dielectric constant material, and the dielectric constant is positively correlated with the amount of dielectric filler added. In addition, the BT nanofiller content has little effect on the dielectric loss (Figure S4), and the dielectric loss remains low for all functional films at frequencies less than 1 MHz. However, the dielectric loss of the functional films was increased when the frequency was higher than 1 MHz. This result indicates that adding BT nanoparticles will improve the performance of the PDMS functional layer, as shown in Figure 3c.

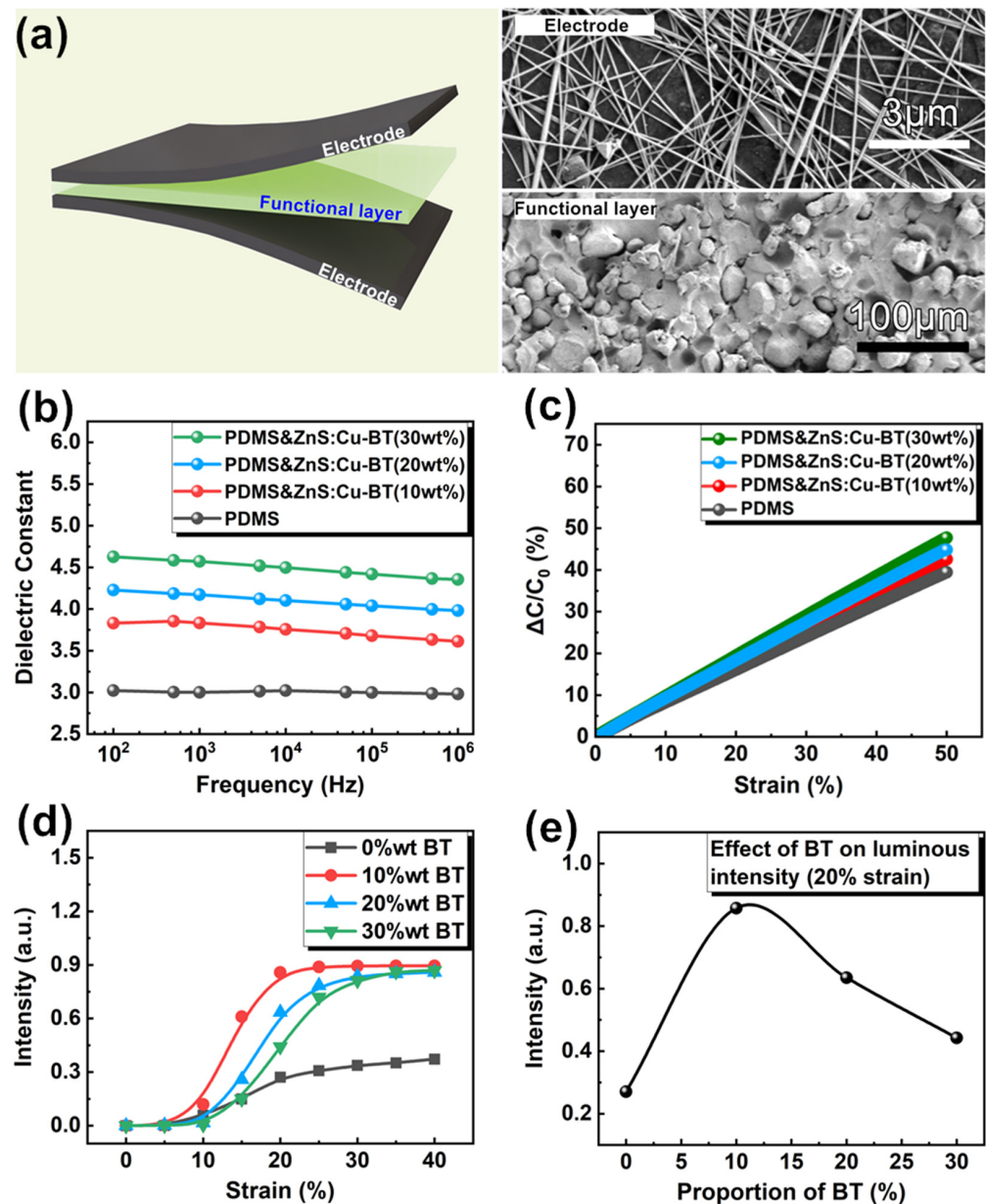


**Figure 3.** Optical and electrical characteristics of e-skin by nanodoped matrix modification. (a) Simplified structure of electronic skin (left), SEM images of the surface morphology of AgNWs/PDMS and cross-sectional morphology of functional layer (right). (b) Frequency dependence of dielectric constant with different BT nanoparticles loading weight fractions (c) Strain dependence of capacitance of strain sensors based on PDMS/ZnS:Cu dielectric layer with different content of BT. (d) The luminescence intensity of the as-prepared sensor with increasing contents of the BT nanoparticle. (e) The luminescence intensity of the as-prepared sensor with different contents of the BT nanoparticle under 20% strain.

In addition, to decide the optimal doping content of BT particles, the following experiments are performed to study the influence of BT doping on the ML intensity. This paper uses the ZnS:Cu microparticles are piezoelectric materials with an asymmetric structure. When mechanical stress is applied to the ZnS:Cu particles, visible light emission is generated because the piezoelectric effect initiates the ML process [23]. As shown in Figure 3d, the functional PDMS layer with ZnS:Cu doping exhibits an ML phenomenon when 5% strain is applied. The doping effect of BT nanoparticles on the ML phenomenon can be seen. By increasing the amount of BT nanoparticles, a significant increase in ML

intensity of the functional layer is observed when the strain is applied in the range from 5% to 40%. Within the 5–40% strain range, the functional films' ML intensity displayed a sharp increase initially, followed by a gradual rise unheld saturation. The saturation ML intensity of the functional layers with BT nanoparticles doping is almost the same and larger than that of the undoped functional layer. It is also observed that the maximum ML intensity is achieved at 10% BT nanoparticles doping amount. Specifically, as shown in Figure 3e, at a particular strain of 20%, the ML intensity of the sensor with BT nanoparticles doping at 10 wt% is 289% stronger than that of the undoped one. When the doping amount of BT nanoparticles exceeds 10%, the ML intensity of the functional layers decreases gradually, yet it remains stronger than without doping. This observation is attributed to the fact that the increased particle density will block and scatter the luminescence. These results indicate that doping by rigid nanoparticles enhances the ML intensity within a specific strain range and boosts the ML intensity saturation value.

Since the functional layer with ZnS:Cu particles and BT nanoparticles are working both as a light-emitting layer and dielectric layer in the proposed sensor, the effect of BT nanoparticles on the capacitive performance and ML intensity of the functional layer should be considered synthetically. The results indicate that although 10 wt% BT nanoparticles doping in the functional layer induced the highest ML intensity, 20 wt% BT nanoparticles doping induced comparable ML intensity. Moreover, further increasing the BT content in this experiment would affect the mechanical properties of the functional layer, so the highest BT loading was kept at 30 wt%. On the other side, the dielectric parameter of the capacitive sensor increases synchronously with the content of BT nanoparticle doping. Therefore, due to its moderate performance, the functional layer with 20 wt% BT content is adopted to prepare the strain sensor.

### 3.4. Electrical Characterization of *e*-Skin

The capacitive performance of the as-prepared sensor is investigated, as shown in Figure 4. As shown in the above section, BT nanoparticle doping is an effective way to increase the dielectric constant of the PDMS film. The dielectric constant of the PDMS film increases as the amount of BT added increases. Afterwards, the functional layers with 20 wt% BT nanoparticles content are used on the sensor to assess its sensitivity. The sensitivity of the capacitive sensor is often evaluated by gauge factor (GF), which is described as the ratio of the measured relative change of electrical signal versus the applied strain:

$$GF = \frac{\Delta C}{C_0 \varepsilon} \quad (2)$$

where  $\Delta C$  is a change of the capacitive signal,  $C_0$  is the initial capacitive signal at strain  $\varepsilon = 0\%$ , and  $\varepsilon$  is the applied strain. To obtain the gauge factor, continuous external strain is applied to the capacitive strain sensors and the capacitive signal is measured. As shown in Figure 4a, the relative capacitance change  $\frac{\Delta C}{C_0}$  ( $C_0$  defined as the original capacitance of the device) of the as-prepared sensor is presented in Figure 4a, which shows an approximately linear relationship between  $\frac{\Delta C}{C_0}$  and applied strain  $\varepsilon$  in the range of 0–50%. The strain sensors presented a GF of 0.9 and a stretchability of 50%. The sensor with 20 wt% BT nanoparticles doping functional layer shows a GF value of 0.9. The achieved GF is close to the record value in CNTs–Ecoflex strain sensors(1, over the strain range up to 150%) [28], CNTs–silicone elastomer(0.99, for strain up to 100%) [29] and higher than AgNWs–Ecoflex strain sensors(0.7, for strain up to 50%) [30]. This work could achieve higher GF by further increasing the effective dielectric constant. However, due to the sensing mechanisms of the capacitive sensor, the GF of the sensor is much less than that of current high-performance resistive strain sensors [31].

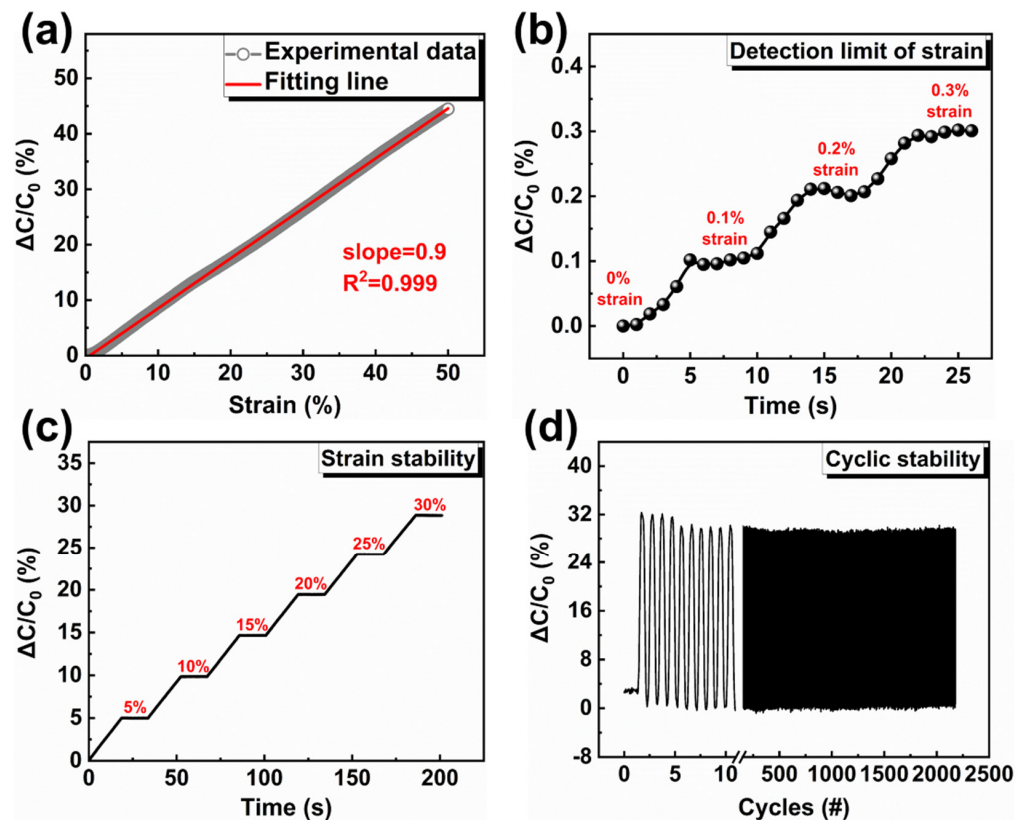


**Figure 4.** Performance characterization of capacitance sensor with 20% BT contents in the dielectric layer. (a) relative capacitance changes versus tensile strain for stretching. (b) Relative capacitance change of the strain sensor upon small strains (from 0.1 to 0.3%). (c) relative capacitance changes of the strain sensor under stretching-holding (0–30%). (d) Response stability of the sensor after 2100 cycles from 0 to 30% strain test.

In addition, the strain sensor reported in this paper showed great linearity in the whole detection range. The linear performance of the capacitive value with increasing strain is mainly due to the thin nature of stretchable electrodes and the softness of the electrode and functional dielectric layer. Furthermore, the Poisson's ratio of the electrode is approximately equal to that of the functional layer. Therefore, the capacitance value varies with the strain under uniaxial tension, and  $\frac{\Delta C}{C_0}$  increases linearly. In general, measuring 30% tensile strain is sufficient for applications of human-related tactile sensing [32]. And the e-skin shows remarkable sensing performance in this strain range.

Moreover, the effect of the dielectric constant of the dielectric layer on the performance of the capacitive strain sensor is also examined. As the dielectric constant of the functional layer increases, the strain sensors show the GF value of 0.85, 0.90, and 0.96 for functional layers with 10 wt%, 20 wt% and 30 wt% of BT nanoparticles doping, respectively. The sensors with higher BT nanoparticle doping have higher GF values, which is mainly attributed to the fact that the doping of BT nanoparticles improves the capacity of the functional layer via modification of the conductivity of the PDMS layer, increasing the effective dielectric constant. Compared to the sensor sandwiched with a pure PDMS dielectric layer, the GF of the sensor with a high dielectric constant dielectric layer is significantly increased across the strain response range. This suggested that higher GF of the sensor can be achieved by adjusting the dielectric constant of the dielectric layer.

In Figure 4b, the detection limit of the sensor is studied. A detectable signal is derived when 0.1% stretched strain is applied, indicating a remarkable detection limit. The stability of the sensor is shown in Figure 4c,d, by monitoring the relative change of the capacitance during stretching. Firstly, the stability of the sensor performance under different strain



states is examined (Figure 4c). No decline in the relative capacitive value is observed when each strain stated is kept for 20 s. It is shown that the capacitive sensor unit has a low response/recovery time small than 20 ms (Figure S6). When the sensor units are integrated into the array on a large scale, the response/recovery time will be extended due to the scanning reading of electrical signals in the array. Moreover, negligible fluctuation in capacitance changes is observed after stretching and releasing over 2100 cycles with 30% tensile strains (Figure 4d), indicating the stability of the sensor.

### 3.5. Optical Characterization of e-Skin

The luminescent intensity was very sensitive to the applied tension on the as-prepared sensor (Figure 5a,b). Both strain and strain rate will influence the ML intensity. A periodic stretching strain was applied to the as-prepared sensor with the layer doped with 20 wt% BT. Indeed, as the strain increased from 10 to 40% (velocity, 600 mm/min), the luminescence intensity was enhanced by a factor of 5. This enhancement is attributed to high stretching tension favours the generation of high-density triboelectric charges. As a result, a high electric field can be obtained to excite the luminescence. As the pressure surpassed 40%, the luminescence intensity tended to saturate, probably because the triboelectric charges density reached a maximum limit.

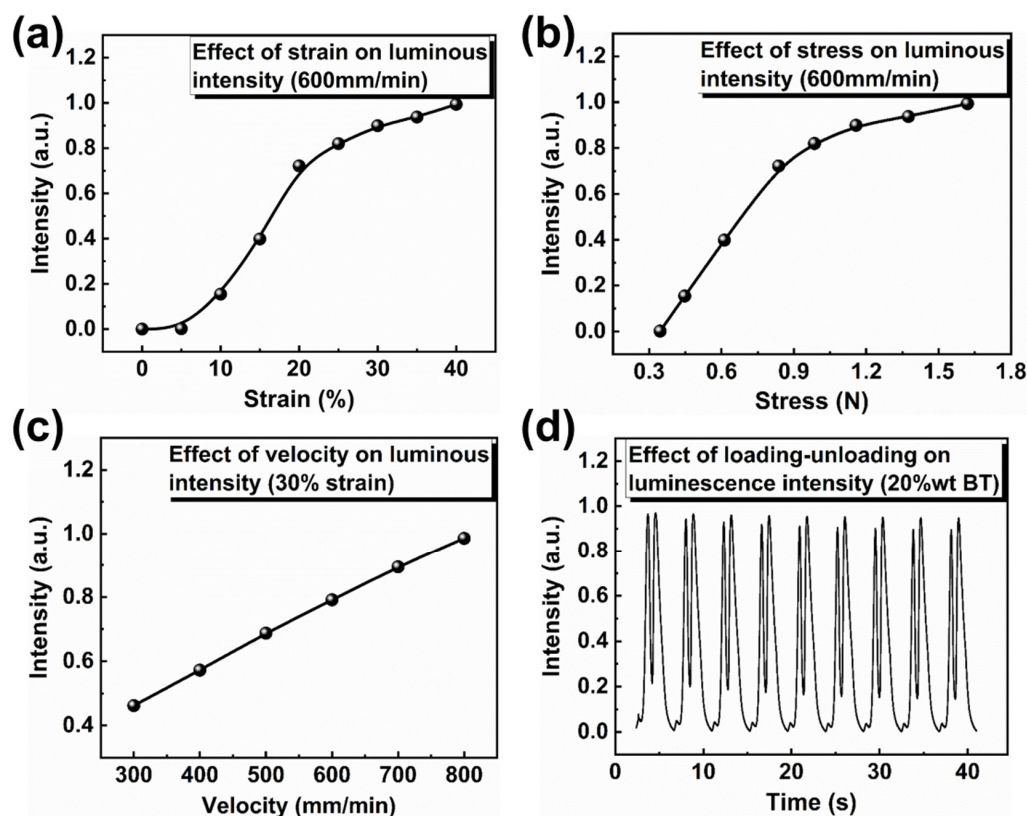


**Figure 5.** Optical characteristics of the ML from the 20% BT nanodoped e-skin. (a) Luminescence intensity as the strain varies from 0 to 40% under 600 mm/min. (b) Luminescence intensity as the stress varies from 0.44 N to 1.62 N under 600 mm/min. (c) Luminescence spectra as the velocity of the tensile strain varies. (d) Stability and repeatability test of ML emitting by nine cycles under 0–30% stretching and releasing.

The correspondence of ML intensity to stress was investigated as well. The function of the stress induced by the press is similar to that of tension induced by strain. Figure 5b presents the plot of the ML intensity (normalized intensity) versus stress, with stress varying from 0.3 N to 1.6 N. Like the plot in Figure 5a, the ML intensity increased with increased applied stress. It tended to saturate when the applied stress was more than

0.9 N. In addition, the correspondence of ML intensity to strain rate was investigated. A linear motor, by which the stretching speed could be precisely controlled, was adopted to apply strain with different strain rates to the sensor. As shown in Figure 5c, the strain rate influenced the luminescence intensity strongly. The ML intensity had a positive linear correlation with the strain rate. From 300 mm/min to 800 mm/min, when the maximum strain is set as 30%, the intensity is increased by 1.2 times. ML's response and recovery time are 0.12 s and 0.19 s, respectively (Figure S7). The response and recovery time of ML mode sensing does not increase with its large-scale integration. Therefore, sensors based on ML mode are suitable for dynamic and large-scale strain detection. This observation was consistent with previous reports [22]. It is indicated that getting the strain and strain rate from the ML intensity is difficult, which limits the ML sensor on precise sensing of the stretching process. However, with the aid of a capacitive sensor, once the information on the maximum strain of the stretching process is given, the ML sensor will provide an efficient way to monitor the dynamic motion process by sensing the strain rate.

The stability of the luminescence was examined by stretching and releasing the as-prepared sensor in several cycles. Interestingly, in each stretching and releasing process, two peaks of luminescence were observed, respectively. It can be explained by the fact that tension and stress induce the ML phenomenon. The mechanoluminescence of ZnS: Cu is caused by the stressing stimuli from BT nanoparticles and the PDMS matrix. The stimuli can be generated during both stretching and releasing processes. The left and right peaks are attributed to the luminescence produced by the stretching and releasing processes. As shown in Figure 5d, no luminescence degradation has been observed in these cycles, indicating the robustness of the sensor and the uniformity and integration of the PDMS and the functional additive.

### 3.6. Demonstration

Due to these excellent properties, the e-skin has promising applications for detecting the motion of human activities, such as sensing joint movements and strain spatial distribution. Therefore, the e-skin based on a capacitive unit and a functional layer was prepared and attached to a glove for real-time monitoring of finger bending motion. As shown in Figure 6a1, the impedance analyzer was used to record the capacitance changes resulting from bending the finger joint three times at each different degree of flexion. As a result, it can be seen that the capacitance value accurately and consistently reflects the bending degree of the finger. Meanwhile, the high-resolution camera captured the ML generated by the finger's dynamic bending (Figure S8).

The corresponding 2D distribution of the relative ML intensity was derived by extracting the gray scale of the captured image to reflect the strain distribution of the skin at the finger joint, as shown in Figure 6a2. It can be seen that the ML intensity is stronger in the middle of the joint than in the area around it, which provide an efficient way to monitor the strain in a large area with high resolution. These are of greater significance in analysing the overall strain applied to the finger.

In addition, a  $10 \times 10$  capacitive array is prepared by patterning electrodes into 100 separated square pixels, each with a size of  $1 \times 1$  mm and a spacing of 1 mm. As shown in Figure 6b1, the e-skin was clamped by two hollow pieces of cardboard and placed above an open beaker. Then, a circular cap is pressed on the surface of the e-skin to induce stress. The actual strain distribution due to the pressing was obtained from the optical platform, as shown in Figure 6b2. For the detection of the e-skin, the relative change in capacitance due to the press was measured by a homemade multi-channel data acquisition system. As shown in Figure 6b3, where the brighter colors correspond to higher capacitance changes, it can be seen from the figure that the pressing leads to a circular-shaped strain distribution. Therefore, an accurate spatial strain distribution was obtained from such a change in the capacitance array.

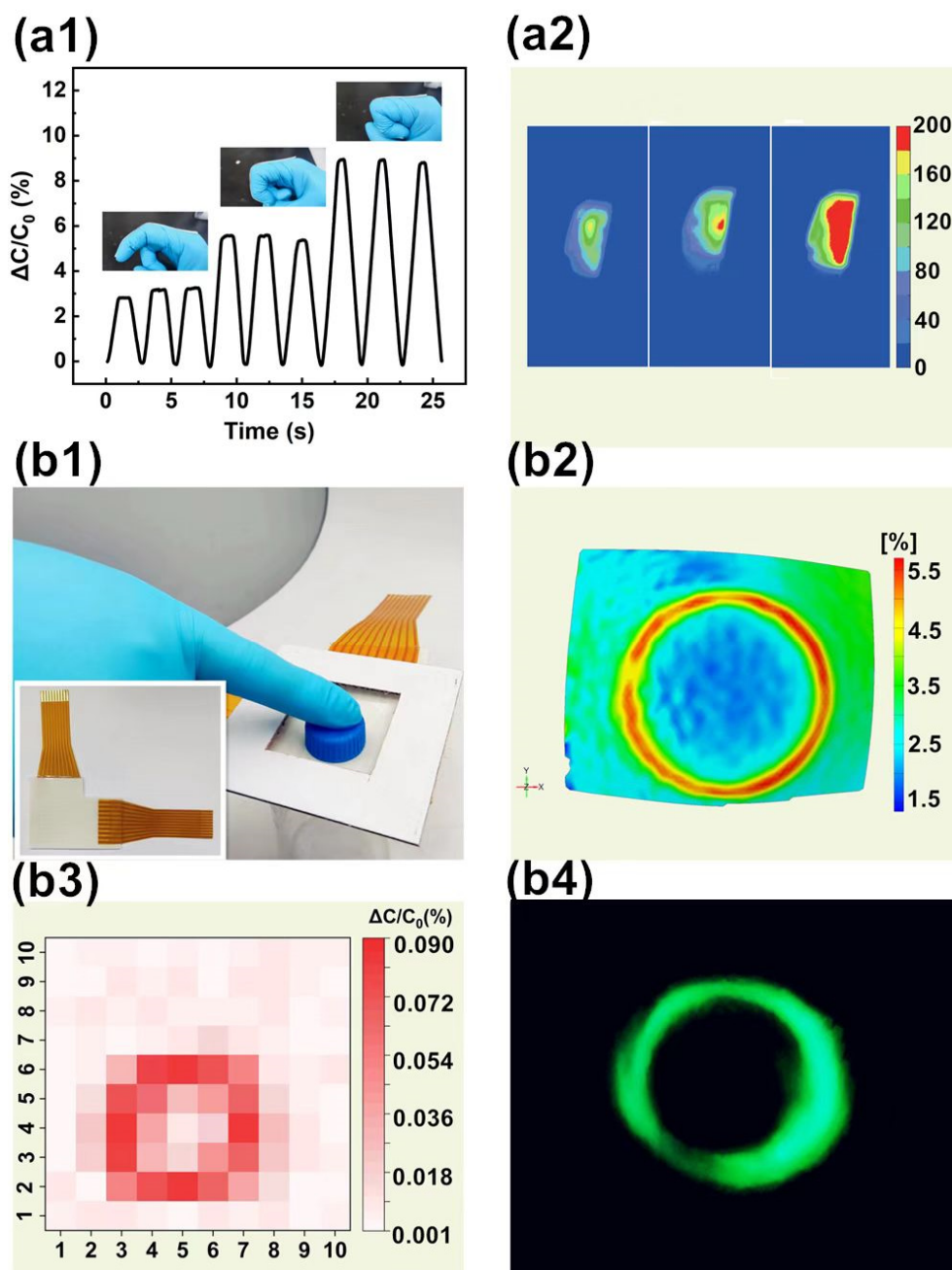


**Figure 6.** Application of e-skin for monitoring of various strains as well as strain distribution sense. (a1) Response capacitance change of the sensor induced by the bending of fingers. Inset: Graph showing a sensor pasted on the finger with increasing bending degree. (a2) The grayscale of the real-time captured image from the ML emission generated by the same three bending degrees. (b1) Schematic diagram of the pressing in strain distribution tests. Inset: Photography of the sensor array based on the e-skin. strain distribution generated by (b2) the Optical platform, (b3) the Capacitive sensor array and (b4) The image of real-time ML in the dark.

Meanwhile, ML images of the dynamic pressing process were taken using the camera, as shown in Figure 6b4, showing a visible green glowing ring, which corresponds strongly to the circle obtained from the capacitance array. The strain record obtained from the capacitance and ML images has an accurate and high-resolution spatial distribution, strongly correlated with the real strain distribution shown in Figure 6b2 generated by the optical platform. It makes the array-integrated e-skin of extraordinary significance for detecting

static and dynamic strain spatial distributions over large areas. These results show that the device has great potential for human motion modeling and practical human interaction, among others.

#### 4. Conclusions

In summary, we have proposed a strain sensor that combines ML with capacitive sensors to accurately detect small-scale strain and high-resolution visualization of large-scale strain in real time. The device features fast dynamic response by generating visualized light signals and accurate static response and feedback with capacitive signals. Additionally, modified BT particles incorporated into the elastic matrix enable stress transfer during stretching, resulting in stronger light emission under the same strain than undoped ones. The doping nanoparticle BT also increases the GF value by boosting the dielectric constant of the capacitive sensor. The ML component and the capacitive sensor showed good stability and durability in the test, with a linear relationship between signal intensity and strain range. This device can be attached to the finger joint to detect the accurate bending degree of the finger and the strain distribution at the finger joint. Furthermore, the sensor array demonstrated unique high-resolution under large-scale strain detection. With its excellent performance and simple manufacturing scheme, this device has great potential for applications in wearable electronics, sports and health monitoring, and human-computer interaction.

**Supplementary Materials:** The following supporting information can be downloaded at: <https://www.mdpi.com/article/10.3390/chemosensors11050270/s1>, Figure S1: Surface of BaTiO<sub>3</sub> is branched with vinyl groups; Figure S2: Chemical reaction of modified BaTiO<sub>3</sub> with PDMS precursor solution; Figure S3: The SEM and EDS image of the cross-sectional of PDMS/ZnS:Cu-BT composite film. (a)(b)(c) Unmodified BT composite film; (d)(e)(f) Modified BT composite film; Figure S4: Dielectric loss of with different BT nanoparticles loading weight fractions; Figure S5: Load-unload cycle curve of e-skin; Figure S6: Response time and recovery time of capacitive strain sensor unit; Figure S7: Response time and recovery time of ML; Figure S8: ML images generated by dynamic bending the finger.

**Author Contributions:** Conceptualization, J.S. and X.Y.; methodology, J.S. and Y.Z.; formal analysis, S.W., Z.G., Z.X., Y.W. (Yuwei Wang) and Y.W. (Yuanzhao Wu); investigation, S.W., Z.X., Z.G. and Y.W. (Yuwei Wang); data curation, S.W., Y.Z. and Z.X.; writing—original draft preparation, S.W., Z.G., Z.X. and Y.W. (Yuanzhao Wu); Writing—review and editing, J.S., X.Y., Y.L. and R.-W.L.; visualization, S.W.; supervision, J.S., R.-W.L.; funding acquisition, J.S., R.-W.L. All authors have read and agreed to the published version of the manuscript.

**Funding:** This research was partially supported by the National Natural Science Foundation of China (U22A20248, 52127803, 51931011, 51971233, 62174165, M-0152, U20A6001, U1909215 and 52105286, 52201236, 62204246, 92064011, 62174164), the External Cooperation Program of Chinese Academy of Sciences (174433KYSB20190038, 174433KYSB20200013), the Instrument Developing Project of the Chinese Academy of Sciences (YJKYYQ20200030), K.C. Wong Education Foundation (GJTD-2020-11), Chinese Academy of Sciences Youth Innovation Promotion Association (2018334), “Pioneer” and “Leading Goose” R&D Program of Zhejiang(2022C01032), Zhejiang Provincial Key R&D Program(2021C01183), Natural Science Foundation of Zhejiang Province (LD22E010002), Zhejiang Provincial Basic Public Welfare Research Project (LGG20F010006), Ningbo Scientific and Technological Innovation 2025 Major Project (2019B10127, 2020Z022), Ningbo Natural Science Foundations (20221JCGY010312).

**Institutional Review Board Statement:** Not applicable.

**Informed Consent Statement:** Not applicable.

**Data Availability Statement:** Not applicable.

**Conflicts of Interest:** The authors declare no conflict of interest.

## References

1. Yang, J.C.; Mun, J.; Kwon, S.Y.; Park, S.; Bao, Z.; Park, S. Electronic Skin: Recent Progress and Future Prospects for Skin-Attachable Devices for Health Monitoring, Robotics, and Prosthetics. *Adv. Mater.* **2019**, *31*, 1904765. [[CrossRef](#)] [[PubMed](#)]
2. Li, W.; Dong, J.; Zhang, X.; Fan, F.R. Recent Progress in Advanced Units of Triboelectric Electronic Skin. *Adv. Mater. Technol.* **2023**, *8*, 2200834. [[CrossRef](#)]
3. Nie, B.; Liu, S.; Qu, Q.; Zhang, Y.; Zhao, M.; Liu, J. Bio-inspired flexible electronics for smart E-skin. *Acta Biomater.* **2022**, *139*, 280–295. [[CrossRef](#)]
4. Wu, S.; Moody, K.; Kollipara, A.; Zhu, Y. Highly Sensitive, Stretchable, and Robust Strain Sensor Based on Crack Propagation and Opening. *ACS Appl. Mater. Interfaces* **2023**, *15*, 1798–1807. [[CrossRef](#)] [[PubMed](#)]
5. Park, J.W.; Kim, T.; Kim, D.; Hong, Y.; Gong, H.S. Measurement of finger joint angle using stretchable carbon nanotube strain sensor. *PLoS ONE* **2019**, *14*, e0225164. [[CrossRef](#)]
6. Guo, J.J.; Guo, C.X.; Zhou, J.L.; Duan, K.; Wang, Q.N. Flexible Capacitive Sensing and Ultrasound Calibration for Skeletal Muscle Deformations. *Soft Robot.* **2022**. *Online Ahead of Print*. [[CrossRef](#)] [[PubMed](#)]
7. García Núñez, C.; Manjakkal, L.; Dahiya, R. Energy autonomous electronic skin. *Npj Flex. Electron.* **2019**, *1*, 1. [[CrossRef](#)]
8. Du, H.; Zhou, H.; Wang, M.; Zhao, G.; Jin, X.; Liu, H.; Chen, W.; Weng, W.; Ma, A. Electrospun Elastic Films Containing AgNW-Bridged MXene Networks as Capacitive Electronic Skins. *ACS Appl. Mater. Interfaces* **2022**, *14*, 31225–31233. [[CrossRef](#)]
9. Meng, H.L.; Zhu, W.H.; Zhou, L.X.; Qian, X.; Bao, G.J. A 3-D Force Sensor Based on Combination of Magnetic and Piezoresistive Transduction. *IEEE Sens. J.* **2022**, *22*, 3595–3604. [[CrossRef](#)]
10. Yuan, H.; Lei, T.; Qin, Y.; Yang, R. Flexible electronic skins based on piezoelectric nanogenerators and piezotronics. *Nano Energy* **2019**, *59*, 84–90. [[CrossRef](#)]
11. Wang, X.; Song, W.Z.; You, M.H.; Zhang, J.; Yu, M.; Fan, Z.; Ramakrishna, S.; Long, Y.Z. Bionic Single-Electrode Electronic Skin Unit Based on Piezoelectric Nanogenerator. *ACS Nano* **2018**, *12*, 8588–8596. [[CrossRef](#)] [[PubMed](#)]
12. Deng, C.; Lan, L.; He, P.; Ding, C.; Chen, B.; Zheng, W.; Zhao, X.; Chen, W.; Zhong, X.; Li, M.; et al. High-performance capacitive strain sensors with highly stretchable vertical graphene electrodes. *J. Mater. Chem. C* **2020**, *8*, 5541–5546. [[CrossRef](#)]
13. Wang, J.; Xu, J.M.; Chen, T.; Song, L.L.; Zhang, Y.L.; Lin, Q.H.; Wang, M.J.; Wang, F.X.; Ma, N.H.; Sun, L.N. Wearable human-machine interface based on the self-healing strain sensors array for control interface of unmanned aerial vehicle. *Sens. Actuators A-Phys.* **2021**, *321*, 112583. [[CrossRef](#)]
14. Angeli, M.A.C.; Caronna, F.; Cramer, T.; Gastaldi, D.; Magagnin, L.; Fraboni, B.; Vena, P. Strain Mapping Inkjet-Printed Resistive Sensors Array. *IEEE Sens. J.* **2020**, *20*, 4087–4095. [[CrossRef](#)]
15. Zymelka, D.; Togashi, K.; Ohigashi, R.; Yamashita, T.; Takamatsu, S.; Itoh, T.; Kobayashi, T. Printed strain sensor array for application to structural health monitoring. *Smart Mater. Struct.* **2017**, *26*, 105040. [[CrossRef](#)]
16. Li, M.; Chen, S.J.; Fan, B.Y.; Wu, B.Y.; Guo, X.J. Printed Flexible Strain Sensor Array for Bendable Interactive Surface. *Adv. Funct. Mater.* **2020**, *30*, 2003214. [[CrossRef](#)]
17. Gu, M.; Li, X.P.; Cao, Y.Y. Optical storage arrays: A perspective for future big data storage. *Light-Sci. Appl.* **2014**, *3*, e177. [[CrossRef](#)]
18. Jeong, S.M.; Song, S.; Joo, K.I.; Kim, J.; Hwang, S.H.; Jeong, J.; Kim, H. Bright, wind-driven white mechanoluminescence from zinc sulphide microparticles embedded in a polydimethylsiloxane elastomer. *Energy Environ. Sci.* **2014**, *7*, 3338–3346. [[CrossRef](#)]
19. Zhuang, Y.; Xie, R.J. Mechanoluminescence Rebrightening the Prospects of Stress Sensing: A Review. *Adv. Mater.* **2021**, *33*, e2005925. [[CrossRef](#)] [[PubMed](#)]
20. Chen, Y.; Wei, X.; Li, H.; Fan, Y.; Hu, W.; Zhu, G. Stretchable Hybrid Bilayered Luminescent Composite Based on the Combination of Strain-Induced and Triboelectrification-Induced Electroluminescence. *ACS Omega* **2019**, *4*, 20470–20475. [[CrossRef](#)]
21. Huang, Z.; Chen, B.; Ren, B.; Tu, D.; Wang, Z.; Wang, C.; Zheng, Y.; Li, X.; Wang, D.; Ren, Z.; et al. Smart Mechanoluminescent Phosphors: A Review of Strontium-Aluminate-Based Materials, Properties, and Their Advanced Application Technologies. *Adv. Sci.* **2023**, *10*, e2204925. [[CrossRef](#)]
22. Qian, X.; Cai, Z.; Su, M.; Li, F.; Fang, W.; Li, Y.; Zhou, X.; Li, Q.; Feng, X.; Li, W.; et al. Printable Skin-Driven Mechanoluminescence Devices via Nanodoped Matrix Modification. *Adv. Mater.* **2018**, *30*, e1800291. [[CrossRef](#)] [[PubMed](#)]
23. Wang, X.; Zhang, H.; Yu, R.; Dong, L.; Peng, D.; Zhang, A.; Zhang, Y.; Liu, H.; Pan, C.; Wang, Z.L. Dynamic pressure mapping of personalized handwriting by a flexible sensor matrix based on the mechanoluminescence process. *Adv. Mater.* **2015**, *27*, 2324–2331. [[CrossRef](#)] [[PubMed](#)]
24. Zhao, B.; Wang, F.; Chen, H.Y.; Zheng, L.X.; Su, L.X.; Zhao, D.X.; Fang, X.S. An Ultrahigh Responsivity (9.7 mA W<sup>-1</sup>) Self-Powered Solar-Blind Photodetector Based on Individual ZnO-Ga<sub>2</sub>O<sub>3</sub> Heterostructures. *Adv. Funct. Mater.* **2017**, *27*, 1700264. [[CrossRef](#)]
25. Zhang, X.; Li, Z.; Du, W.; Zhao, Y.; Wang, W.; Pang, L.; Chen, L.; Yu, A.; Zhai, J. Self-powered triboelectric-mechanoluminescent electronic skin for detecting and differentiating multiple mechanical stimuli. *Nano Energy* **2022**, *96*, 107115. [[CrossRef](#)]
26. Mukhina, M.V.; Tresback, J.; Ondry, J.C.; Akey, A.; Alivisatos, A.P.; Kleckner, N. Single-Particle Studies Reveal a Nanoscale Mechanism for Elastic, Bright, and Repeatable ZnS:Mn Mechanoluminescence in a Low-Pressure Regime. *ACS Nano* **2021**, *15*, 4115–4133. [[CrossRef](#)] [[PubMed](#)]
27. Jun, S.Y.; Park, S.H.; Sohn, M.K.; Kim, S.; Lee, J.M.; Kong, D.S.; Lee, T.Y.; Jung, J.H.; Kim, M.S.; Yoo, S.; et al. Reduction time effect on the dielectric characteristics of reduced-graphene-oxide-encapsulated barium titanate powder fillers. *Carbon* **2022**, *199*, 23–32. [[CrossRef](#)]

28. Shin, U.H.; Jeong, D.W.; Park, S.M.; Kim, S.H.; Lee, H.W.; Kim, J.M. Highly stretchable conductors and piezocapacitive strain gauges based on simple contact-transfer patterning of carbon nanotube forests. *Carbon* **2014**, *80*, 396–404. [[CrossRef](#)]
29. Cohen, D.J.; Mitra, D.; Peterson, K.; Maharbiz, M.M. A Highly Elastic, Capacitive Strain Gauge Based on Percolating Nanotube Networks. *Nano Lett.* **2012**, *12*, 1821–1825. [[CrossRef](#)] [[PubMed](#)]
30. Yao, S.; Zhu, Y. Wearable multifunctional sensors using printed stretchable conductors made of silver nanowires. *Nanoscale* **2014**, *6*, 2345–2352. [[CrossRef](#)]
31. Zheng, X.; Wang, Y.; Nie, W.; Wang, Z.; Hu, Q.; Li, C.; Wang, P.; Wang, W. Elastic polyaniline nanoarrays/MXene textiles for all-solid-state supercapacitors and anisotropic strain sensors. *Compos. Part A* **2022**, *158*, 106985. [[CrossRef](#)]
32. Park, S.; Kim, H.; Vosgueritchian, M.; Cheon, S.; Kim, H.; Koo, J.H.; Kim, T.R.; Lee, S.; Schwartz, G.; Chang, H.; et al. Stretchable energy-harvesting tactile electronic skin capable of differentiating multiple mechanical stimuli modes. *Adv. Mater.* **2014**, *26*, 7324–7332. [[CrossRef](#)] [[PubMed](#)]

**Disclaimer/Publisher’s Note:** The statements, opinions and data contained in all publications are solely those of the individual author(s) and contributor(s) and not of MDPI and/or the editor(s). MDPI and/or the editor(s) disclaim responsibility for any injury to people or property resulting from any ideas, methods, instructions or products referred to in the content.